Journal of Computational Physics **182,** 213–233 (2002)
doi:10.1006/jcph.2002.7162

Unconditionally Stable and Robust Adjacent-Cell Diffusive Preconditioning of Weighted-Difference Particle Transport Methods Is Impossible

Y. Y. Azmy[1,2]

Oak Ridge National Laboratory,[3] *P. O. Box 2008, MS 6363, Oak Ridge, Tennessee 37831-6363*
E-mail: yya3@psu.edu

Received January 19, 2002; revised June 24, 2002

We construct a particle transport problem for which there exists no preconditioner with a cell-centered diffusion coupling stencil that is unconditionally stable and robust. In particular we consider an asymptotic limit of the periodic horizontal interface (PHI) configuration wherein the cell height in both layers approaches zero like σ^2 while the total cross section vanishes like σ in one layer and diverges like σ^{-1} as $\sigma \to 0$ in the other layer. In such cases we show that the conditions for stability and robustness of the flat eigenmodes of the iteration residual imply instability of the modes flat in the y-dimension and rapidly varying in the x-dimension. Two assumptions are made in the proof. (i) Only cell-centered adjacent-cell preconditioners (AP) are considered; nevertheless numerical experiments with face-centered preconditioners of the diffusion synthetic acceleration (DSA) type on problem configurations with sharp material discontinuities suffer similar deterioration in spectral properties. (ii) The spatial weights of the arbitrarily high-order transport method of the nodal type and zeroth order (AHOT-N0) are used in the analysis; nevertheless similar results are expected for alternative spatial approximation methods as long as their spatial weights continuously approach the correct asymptotic limits: 0 and 1 for thin and thick cells, respectively. The result of the proof is verified by solving a finite approximation of PHI with three existing codes, two of which are not constrained by these assumptions. The spectral radii reported by the three codes behave as predicted by our analysis, i.e., reaching values that far exceed the maximum spectral radii determined via homogeneous model configuration analysis. This constitutes preliminary

[1] The submitted manuscript has been authored by a contractor of the U.S. Government under Contract DE-AC05-00OR22725.

[2] Permanent address: The Pennsylvania State University, 229 Reber Building, University Park, Pennsylvania 16802.

[3] Oak Ridge National Laboratory is managed by UT–Battelle, LLC, for the U.S. Department of Energy under Contract DE-AC05-00OR22725.

0021-9991/02 $35.00
Published by Elsevier Science (USA)

evidence that our conclusions might extend to a wider class of transport methods and acceleration schemes than is considered in the analysis.

Key Words: iterative acceleration; diffusive preconditioners; neutral particle transport; unconditional; stability; robustness.

1. INTRODUCTION

The need for accelerating source iterations used in particle transport calculations has long been recognized [1–3]. Significant effort has been invested in identifying the problems most in need of acceleration and in developing stable and robust acceleration schemes for them [4]. Among the most popular techniques has been the diffusion synthetic acceleration (DSA) method, which for model problems, i.e., uniform mesh and homogeneous material composition, is unconditionally stable and robust [2, 3]. (In this paper we employ the standard meaning of the term *stable*, namely iterative convergence for arbitrary initial guess; the term *robust* implies convergence in a number of iterations that does not increase with problem size. Hence stability requires the spectral radius to be smaller than 1, while robustness requires it to be significantly smaller than 1, independent of problem size.) More recently the adjacent-cell preconditioner scheme was devised to address some of the limitations of DSA in multidimensional geometry [5–7]. Namely, AP applies a cell-centered diffusion coupling stencil, thus comprising a smaller algebraic system than does face-centered DSA, and achieves better spectral properties in model problem configurations [5]. By definition AP includes cell-centered DSA schemes as special cases, but it is not constrained in the choice of the diffusion parameters except to require stability of the accelerated iterations. Spectral analysis of AP predicted its unconditional stability and robustness, i.e., a spectral radius significantly smaller than 1, for model problems over a wide range of problem parameters, in particular cell size and total cross section [5–7]. Furthermore, test problems with sharp mesh and material discontinuities demonstrated the robustness of AP in slab geometry in such instances [5]. In contrast, in multidimensional non-model problems AP with a reciprocal-averaging mixing formula suffered significant inefficiency with increasing discontinuity in the total cross section [6, 7].

It was initially suspected that the reason for AP's inefficiency is a coding bug, a numerical artifact, or an indication of the inadequacy of the reciprocal-averaging mixing formula. The first two possibilities were eliminated by conducting a Fourier analysis of AP with the reciprocal-averaging mixing formula on the periodic horizontal interface (PHI) configuration and analytically predicting the effect of the magnitude of material heterogeneity on stability and robustness [8]. The PHI configuration is composed of two types, $j = 1, 2$, of infinite horizontal stripes one cell thick each, stacked on top of one another so that every stripe of type 1(2) is sandwiched between two stripes of type 2(1), respectively. Thus the horizontal interface separating stripe types 1 and 2 repeats periodically along the y-dimension [8]. Many attempts then were made to find a better, unconditionally stable mixing formula for the PHI configuration with no success [8], and the question became whether there is *any* preconditioner with a diffusion stencil that possesses this property. In this paper we show that no such preconditioner exists. Our conclusion extends beyond AP to include all cell-centered diffusion operators, and based on numerical experiments we conjecture it will also hold for face-centered schemes. Also, while the analysis presented here is performed for the arbitrarily high-order transport method of the nodal type and order 0 (AHOT-N0)

[9], which continuously spans the entire range of cell sizes with the correct limits of the spatial weights, our conclusion is valid for all spatial discretizations of S_n methods that possess correct limits of the spatial weights, namely diamond difference (DD) and step for thin and thick cells, respectively. [AHOT-N0 is also known as the zeroth-order nodal integral method (0NIM) in the literature.]

In Section 2 we present a spectral analysis of the source iterations (SI) for the AHOT-N0 using the PHI configuration and observe the effect of material discontinuity on the spectrum. The stability of a generic AP-accelerated scheme is investigated in Section 3 and two alternative stability conditions are derived. We use these stability conditions in Section 4 to show that for an asymptotic realization of PHI any choice of the acceleration operator parameters will cause either (a) the flat mode eigenvalue to approach unity or (b) the eigenmode that is flat in y and high frequency in x to become unstable. This is done for arbitrary preconditioner parameters, implying the impossibility of simultaneous unconditional stability and robustness for any preconditioner with this coupling stencil. Since viable acceleration schemes cannot be designed to include a known instability, only preconditioners that suffer the above symptom (a) in the PHI configuration are worthy of consideration. While not unconditionally robust, in the PHI configuration these methods still converge faster than SI because their spectral radius is smaller than, albeit approaching, unity.

The analysis presented in this paper is verified numerically in Section 5 via three codes based on different transport methods and acceleration schemes, two of which go beyond the limitations imposed by the analysis, thus suggesting that this result might apply to a broader class of methods than has been proven here. A brief discussion of the results and conclusions of this work is included in Section 6.

2. SPECTRAL ANALYSIS OF THE SOURCE ITERATIONS

We start by analyzing the iterative convergence of SI for AHOT-N0 in order to introduce the notation and to develop some expressions for later use in this paper. The discrete variable equations for the AHOT-N0 in two-dimensional Cartesian geometry written in weighted diamond difference (WDD) form are comprised of one balance equation per discrete ordinate, per computational cell, j,

$$\frac{\epsilon_j^x}{2}\left(\psi_{+j}^{\ y}-\psi_{-j}^{\ y}\right)+\frac{\epsilon_j^y}{2}\left(\psi_{+j}^{\ x}-\psi_{-j}^{\ x}\right)+\bar{\psi}_j=c_j\bar{\Phi}_j^{\ell}, \tag{1}$$

and one weighted-difference relation per discrete ordinate, per cell, per dimension, e.g.,

$$\bar{\psi}_j=\left(\frac{1+\alpha_j^x}{2}\right)\psi_{+j}^{\ y}+\left(\frac{1-\alpha_j^x}{2}\right)\psi_{-j}^{\ y}, \tag{2}$$

with an analogous expression in the y-dimension [9]. In Eqs. (1) and (2) we used standard notation [9]: c_j is the scattering ratio in cell j;

$$\epsilon_j^x\equiv\frac{2|\mu|}{\sigma_j a_j},\quad \epsilon_j^{\ y}\equiv\frac{2|\eta|}{\sigma_j b_j}, \tag{3}$$

where μ and η are the discrete ordinate's direction cosines with respect to the x- and y-axes, respectively; σ_j is the macroscopic total cross section in cell j; and a_j and b_j denote the cell size in the x- and y-dimensions, respectively.

In the standard form of the discrete variable transport equation, $\bar{\psi}_j$ and $\bar{\phi}_j^\ell$ denote the angular flux and ℓth iterate of the scalar flux, respectively, averaged over cell j; ψ_{+j}^{y} and ψ_{-j}^{y} denote the angular flux averaged over the outgoing and incoming, respectively ℓ, $x = const$ faces of cell j, with analogous difinitions for $\psi_{\pm j}^{x}$. However, for the benefit of the Fourier analysis to be conducted shortly, Eq. (1) is written in the homogeneous form, i.e., with no distributed source, implying that the flux variables in Eqs. (1) and (2) actually denote iteration residuals. For AHOT-N0 the spatial weights [9]

$$\alpha_j^x \equiv \coth\left(1/\epsilon_j^x\right) - \epsilon_j^x, \quad \alpha_j^y \equiv \coth\left(1/\epsilon_j^y\right) - \epsilon_j^y \tag{4}$$

vary continuously from the DD value of 0 for thin cells to the step method value of 1 for thick cells. Note that in Eqs. (1) and (2) the discrete ordinate and iteration indices on the angular flux discrete variables, and in Eqs. (3) and (4) the discrete ordinate index on angle-dependent parameters, have been suppressed.

The mesh-sweep iteration residual of the scalar flux is computed from

$$\tilde{\phi}_j^\ell = \sum_{\mu,\eta} \omega \bar{\psi}_j, \tag{5}$$

and the SI update formula amounts to

$$\bar{\phi}_j^{\ell+1} = \tilde{\phi}_j^\ell. \tag{6}$$

Without any loss of generality we can assume that in PHI the cell thickness in the x-direction is $a_1 = a_2 = 1$; otherwise the total cross sections σ_1 and σ_2 can be scaled to this effect. The standard approach for determining the spectrum of iterative schemes typically applies to a model configuration composed of an infinite uniform mesh and a single, homogeneous material. The iterates, hence the solution, of the discrete variables in such configurations possess spatial periodicity in multiples of the mesh size that permits decomposition into Fourier modes. Orthogonality of the Fourier modes permits their separation so that each mode can be considered separately, providing an expression for the iteration eigenvalue in terms of the problem parameters. The same principles are applicable in the PHI configuration, except that in the y-dimension the periodicity is in multiples of $b_1 + b_2$, and the variables in each layer are decomposed separately. Thus we introduce the Fourier decomposition, with the origin arbitrarily set at the center of a cell in one of the layers $j = 1$:

$$\bar{\phi}_1^\ell(x, y) = \bar{\Phi}_1^\ell e^{\hat{\imath}[\lambda_x x + \lambda_y y]}, \tag{7a}$$

$$\bar{\phi}_2^\ell(x, y) = \bar{\Phi}_2^\ell e^{\hat{\imath}[\lambda_x x + \lambda_y (y + \mathrm{sg}(\eta)(b_1+b_2)/2)]}, \tag{7b}$$

$$\tilde{\phi}_1^\ell(x, y) = \tilde{\Phi}_1^\ell e^{\hat{\imath}[\lambda_x x + \lambda_y y]}, \tag{7c}$$

$$\tilde{\phi}_2^\ell(x, y) = \tilde{\Phi}_2^\ell e^{\hat{\imath}[\lambda_x x + \lambda_y (y + \mathrm{sg}(\eta)(b_1+b_2)/2)]}, \tag{7d}$$

$$\bar{\psi}_1(x, y) = \bar{\Psi}_1 e^{\hat{\imath}[\lambda_x x + \lambda_y y]}, \tag{7e}$$

$$\bar{\psi}_2(x, y) = \bar{\Psi}_2 e^{\hat{\imath}[\lambda_x x + \lambda_y (y + \mathrm{sg}(\eta)(b_1+b_2)/2)]}, \tag{7f}$$

$$\psi_{+1}^{x}(x, y) = \Psi^x e^{\hat{\imath}[\lambda_x x + \lambda_y (y - \mathrm{sg}(\eta) b_1/2)]}, \tag{7g}$$

$$\psi^x_{-2}(x, y) = \Psi^x e^{\hat{\imath}[\lambda_x x + \lambda_y (y + \mathrm{sg}(\eta)(b_1/2 + b_2))]}, \tag{7h}$$

$$\psi^y_{\pm 1}(x, y) = \Psi^y_1 e^{\hat{\imath}[\lambda_x (x \mp \mathrm{sg}(\mu)/2) + \lambda_y y]}, \tag{7i}$$

$$\psi^y_{\pm 2}(x, y) = \Psi^y_2 e^{\hat{\imath}[\lambda_x (x \mp \mathrm{sg}(\mu)/2) + \lambda_y (y + \mathrm{sg}(\eta)(b_1 + b_2)/2)]}. \tag{7j}$$

Note that the subscripts 1 and 2 now refer to the corresponding layer in the PHI configuration, not to a specific cell as in Eqs. (1), (2), and (6). In Eqs. (7) uppercase symbols denote the Fourier coefficients of the corresponding variable, $\hat{\imath} \equiv \sqrt{-1}$, sg(.) is the signum function, and λ_x, λ_y are the Fourier variables in the x-, y-dimension, respectively. The continuity of the flux on the interface between materials 1 and 2, i.e., $\psi^x_{-1} = \psi^x_{+2}$, makes it unnecessary to decompose them into their Fourier modes.

The spectrum of the SI scheme for the PHI configuration is now obtained by substituting Eqs. (7) into Eqs. (1), (2), and (6) for each layer $j = 1, 2$, then eliminating all angular flux variables. This yields the mapping of the eigenmodes of the previous iterate of the scalar flux residual, $\{\bar{\Phi}^\ell_1, \bar{\Phi}^\ell_2\}^T$, into their mesh-sweep counterparts, $\{\tilde{\Phi}^\ell_1, \tilde{\Phi}^\ell_2\}^T$,

$$\begin{bmatrix} \tilde{\Phi}^\ell_1 \\ \tilde{\Phi}^\ell_2 \end{bmatrix} = \mathbf{B} \begin{bmatrix} \bar{\Phi}^\ell_1 \\ \bar{\Phi}^\ell_2 \end{bmatrix}, \tag{8}$$

where

$$\mathbf{B} \equiv \sum_{\mu,\eta} \omega \mathbf{A}^{-1} \mathbf{C}, \tag{9a}$$

$$\begin{aligned} \mathbf{A} \equiv \mathbf{I} &+ \hat{\imath}\,\mathrm{sg}(\mu) \sin r \begin{bmatrix} \epsilon^x_1 / \left(\cos r + \hat{\imath}\,\mathrm{sg}(\mu)\,\alpha^x_1 \sin r\right) & 0 \\ 0 & \epsilon^x_2 / \left(\cos r + \hat{\imath}\,\mathrm{sg}(\mu)\,\alpha^x_2 \sin r\right) \end{bmatrix} \\ &+ \begin{bmatrix} \epsilon^y_1 \left(\cos s + \hat{\imath}\,\mathrm{sg}(\eta)\,\alpha^y_2 \sin s\right) & -\epsilon^y_1 \\ -\epsilon^y_2 & \epsilon^y_2 \left(\cos s + \hat{\imath}\,\mathrm{sg}(\eta)\,\alpha^y_1 \sin s\right) \end{bmatrix} \\ &\div \left[\left(\alpha^y_1 + \alpha^y_2\right) \cos s + \hat{\imath}\,\mathrm{sg}(\eta) \left(1 + \alpha^y_1 \alpha^y_2\right) \sin s \right], \end{aligned} \tag{9b}$$

$$\mathbf{C} \equiv \begin{bmatrix} c_1 & 0 \\ 0 & c_2 \end{bmatrix}, \tag{9c}$$

where $\mathbf{I}$ is the identity matrix and $r \equiv \lambda_x/2$, $s \equiv \lambda_y (b_1 + b_2)/2$.

The rate of convergence of SI is determined by the spectral radius of the $\mathbf{B}$ matrix. For each point in Fourier space, (r, s), $\mathbf{B}$ has two eigenvalues; the supremum of the largest magnitude of these over the entire Fourier space is the spectral radius of SI. Investigating the spectrum of the SI scheme for the PHI configuration we observe significant similarty to the model problem spectrum. Namely, the spectral radius is unity and the slowest converging eigenmodes are the *flattest* modes; i. e., $r, s \sim 0$. One peculiar feature of the PHI case, however, is the diminishing range of the spectrum with increasing material discontinuity whereby for each Fourier mode, r, s, the larger (in absolute value) of the two eigenvalues increases toward unity. In other words, the infimum of the absolute value of the spectrum over the Fourier space approaches its supremum, i. e., unity, as the material discontinuity increases. It follows that the dominance ratio of the fundamental mode approaches unity

and this results in generally slower convergence along a pattern characterized by an initial linear increase in the iteration residual prior to the onset of exponential attenuation.

Acceleration methods generally replace the update formula, Eq. (6), with a more sophisticated, typically coupled, system of equations that aims at reducing the spectral radius of the combined system. Preconditioning provides a general framework for this idea by [6, 7]

$$\bar{\phi}_j^{\ell+1} = \tilde{\phi}_j^{\ell} + \mathbf{D}^{-1}\left(\tilde{\phi}_j^{\ell} - \bar{\phi}_j^{\ell}\right), \tag{10}$$

where $\mathbf{D}$ is a generic preconditioner operator which couples the elements of its operand in a pattern determined by its sparsity. Restricting $\mathbf{D}$ to cell-centered preconditioners that couple only nearest neighbors, e.g., the diffusion coupling scheme, we obtain the class of AP whose representation in Fourier space is given by

$$\mathbf{D}\begin{bmatrix}\bar{\Phi}_1^{\ell}\\ \bar{\Phi}_2^{\ell}\end{bmatrix} = \begin{bmatrix} D_1 + 2D_{x,1}\cos(2r) & 2D_{y,1}\cos(s)\\ 2D_{y,2}\cos(s) & D_2 + 2D_{x,2}\cos(2r)\end{bmatrix}\begin{bmatrix}\bar{\Phi}_1^{\ell}\\ \bar{\Phi}_2^{\ell}\end{bmatrix}, \tag{11}$$

where D_1 and D_2 are the self-coupling elements of $\mathbf{D}$ for cells in stripes 1 and 2, respectively; $D_{x,j}$, $j = 1, 2$, are the coupling elements in the x-dimension for each stripe type j; and $D_{y,j}$ are the elements coupling the scalar flux residual in a cell type j to its value in cell type $j' \neq j$, along the y-dimension. The AP as implemented and tested earlier is based on expressions for the preconditioner elements derived for model problem configuration and mixed via the traditional reciprocal-averaging formula [6, 7]. In contrast, here we leave the preconditioner elements completely arbitrary and independent, i.e., no mixing formula, in a search for values that would render the iterative process for the PHI configuration unconditionally and simultaneously stable and robust.

Decomposing the updating formula, Eq. (10), into Fourier modes and then using Eqs. (8) and (11), we obtain the mapping of the AP-accelerated eigenmodes of the scalar flux residual

$$\vec{\bar{\Phi}}^{\ell+1} = \mathbf{M}\vec{\bar{\Phi}}^{\ell}, \tag{12}$$

where we have defined

$$\vec{\bar{\Phi}}^{\nu} \equiv \left\{\bar{\Phi}_1^{\nu}, \bar{\Phi}_2^{\nu}\right\}^T, \quad \nu = \ell, \ell+1, \tag{13a}$$

$$\mathbf{M} \equiv \mathbf{B} + \mathbf{D}^{-1}(\mathbf{B} - \mathbf{I}). \tag{13b}$$

The spectral radius of matrix $\mathbf{M}$ determines the stability of the accelerated iterations.

3. STABILITY CONDITIONS FOR THE FLAT EIGENMODES

We now study the behavior of $\mathbf{M}$ near the origin in Fourier space and derive stability conditions for the flat eigenmode, $r, s \to 0$. Expanding Eq. (9b) in a truncated series about the origin in Fourier space yields

$$\mathbf{A} \to \mathbf{A}_0 + r\mathbf{A}_r + s\mathbf{A}_s + r^2\mathbf{A}_{r^2} + s^2\mathbf{A}_{s^2}, \tag{14}$$

where

$$\mathbf{A}_0 = \mathbf{I} + \frac{1}{\alpha_1^y + \alpha_2^y}\begin{bmatrix}\epsilon_1^y & -\epsilon_1^y\\ -\epsilon_2^y & \epsilon_2^y\end{bmatrix}, \tag{15a}$$

$$\mathbf{A}_r = \hat{\imath}\mathrm{sg}(\mu)\begin{bmatrix}\epsilon_1^x & 0\\ 0 & \epsilon_2^x\end{bmatrix}, \tag{15b}$$

$$\mathbf{A}_s = \frac{\hat{\imath}\mathrm{sg}(\eta)}{\left(\alpha_1^y+\alpha_2^y\right)^2}\begin{bmatrix}\epsilon_1^y\left[\left(\alpha_2^y\right)^2-1\right] & \epsilon_1^y\left[\alpha_1^y\alpha_2^y+1\right]\\ \epsilon_2^y\left[\alpha_1^y\alpha_2^y+1\right] & \epsilon_2^y\left[\left(\alpha_1^y\right)^2-1\right]\end{bmatrix}, \tag{15c}$$

$$\mathbf{A}_{r^2} = \begin{bmatrix}\epsilon_1^x\alpha_1^x & 0\\ 0 & \epsilon_2^x\alpha_2^x\end{bmatrix}, \tag{15d}$$

$$\mathbf{A}_{s^2} = \frac{1}{\left(\alpha_1^y+\alpha_2^y\right)^3}\begin{bmatrix}\epsilon_1^y\left(\alpha_1^y\alpha_2^y+1\right)\left[\left(\alpha_2^y\right)^2-1\right] & \epsilon_1^y\left[\left(\alpha_1^y\alpha_2^y+1\right)^2-\frac{1}{2}\left(\alpha_1^y+\alpha_2^y\right)^2\right]\\ \epsilon_2^y\left[\left(\alpha_1^y\alpha_2^y+1\right)^2-\frac{1}{2}\left(\alpha_1^y+\alpha_2^y\right)^2\right] & \epsilon_2^y\left(\alpha_1^y\alpha_2^y+1\right)\left[\left(\alpha_1^y\right)^2-1\right]\end{bmatrix}. \tag{15e}$$

Inverting Eq. (14) and then substituting the resulting series into the definition of $\mathbf{B}$, Eq. (9a), results in a truncated series of the form

$$\mathbf{B} \to \mathbf{B}_0 + r^2\mathbf{B}_{r^2} + s^2\mathbf{B}_{s^2}, \tag{16}$$

where the first-order terms vanish assuming symmetry of the angular quadrature, and where

$$\mathbf{B}_0 = \left\{\sum_{\mu,\eta}\omega\mathbf{A}_0^{-1}\right\}\mathbf{C} = \mathbf{C} + \begin{bmatrix}-E_1 & E_1\\ E_2 & -E_2\end{bmatrix}\mathbf{C}, \tag{17a}$$

$$\begin{aligned}\mathbf{B}_{t^2} &= \left\{\sum_{\mu,\eta}\omega\mathbf{A}_0^{-1}\left(\mathbf{A}_t\mathbf{A}_0^{-1}\mathbf{A}_t - \mathbf{A}_{t^2}\right)\mathbf{A}_0^{-1}\right\}\mathbf{C}\\ &\equiv \begin{bmatrix}\beta_{1,1}^t & \beta_{1,2}^t\\ \beta_{2,1}^t & \beta_{2,2}^t\end{bmatrix}\mathbf{C}, \quad t \equiv r \text{ or } s.\end{aligned} \tag{17b}$$

The elements E_j, $\beta_{j,j'}^t$, $j, j' = 1, 2$ and $t = r$ or s, are obtained by taking the appropriate limits of Eq. (9b). For example,

$$E_j \equiv \sum_{\mu,\eta}\frac{\omega\,\epsilon_j^y}{\epsilon_1^y+\epsilon_2^y+\alpha_1^y+\alpha_2^y}, \quad j = 1, 2. \tag{18}$$

It is easy to show that in case of perfect scattering, $\mathbf{C} = \mathbf{I}$, if the preconditioner is not singular at $r = s = 0$ then the spectral radius of $\mathbf{M}$ is bounded from below by 1, implying lack of robustness. Hence a necessary condition for stability and robustness of the preconditioned iterations is the vanishing of the determinant of $\mathbf{D}$ at the origin in Fourier space,

$$\tilde{D}_1\tilde{D}_2 = 4D_{y,1}D_{y,2}, \tag{19a}$$

$$\tilde{D}_j \equiv D_j + 2D_{x.j}. \tag{19b}$$

To determine the behavior of $\mathbf{D}^{-1}$ near the origin in Fourier space, first we expand $\mathbf{D}$, as defined by Eq. (11), in a truncated series,

$$\mathbf{D} \to \begin{bmatrix}D_1+2D_{x,1} & 2D_{y,1}\\ 2D_{y,2} & D_2+2D_{x,2}\end{bmatrix} - 4r^2\begin{bmatrix}D_{x,1} & 0\\ 0 & D_{x,2}\end{bmatrix} - s^2\begin{bmatrix}0 & D_{y,1}\\ D_{y,2} & 0\end{bmatrix}. \tag{20}$$

Inverting this matrix, then applying the robustness condition, Eq. (19a), produces

$$\mathbf{D}^{-1} \to \frac{1}{\Delta}\begin{bmatrix} \tilde{D}_2 - 4r^2 D_{x,2} & (-2+s^2)D_{y,1} \\ (-2+s^2)D_{y,2} & \tilde{D}_1 - 4r^2 D_{x,1} \end{bmatrix}, \tag{21}$$

where Δ denotes the determinant of the preconditioner near the origin

$$\Delta = -4r^2(\tilde{D}_1 D_{x,2} + \tilde{D}_2 D_{x,1}) + 4s^2 D_{y,1} D_{y,2}. \tag{22}$$

Clearly $\mathbf{M}$ does not exist at the origin [see Eqs. (13b) and (19a)] and only its limit as $r, s \to 0$, $\mathbf{M}^0$, can be considered. Substituting Eqs. (17) and (21) into Eq. (13b), and after some algebra, this limit of the elements of $\mathbf{M}$ becomes

$$M^0_{j,j} \to -\frac{E_j \tilde{D}_{j'} + 2E_{j'} D_{y,j}}{\Delta} + (1 - E_j) + \frac{r^2}{\Delta}\left(\tilde{D}_{j'}\beta^r_{j,j} + 4E_j D_{x,j'} - 2D_{y,j}\beta^r_{j',j}\right) + \frac{s^2}{\Delta}\left(\tilde{D}_{j'}\beta^s_{j,j} + \left(E_{j'} - 2\beta^s_{j',j}\right)D_{y,j}\right) + O(r^2, s^2), \tag{23a}$$

$$M^0_{j,j'} \to \frac{E_j \tilde{D}_{j'} + 2E_{j'} D_{y,j}}{\Delta} + E_j + \frac{r^2}{\Delta}\left(\tilde{D}_{j'}\beta^r_{j,j'} - 4E_j D_{x,j'} - 2D_{y,j}\beta^r_{j',j'}\right) + \frac{s^2}{\Delta}\left(\tilde{D}_{j'}\beta^s_{j,j'} - \left(E_{j'} + 2\beta^s_{j',j'}\right)D_{y,j}\right) + O(r^2, s^2), \quad j, j' = 1, 2. \tag{23b}$$

It is evident that $\mathbf{M}^0$ has two scales near the origin in Fourier space: the first diverges like $O(r^{-2}, s^{-2})$, and the other is $O(1)$. Separating the unbounded component then requiring the $O(r^{-2}, s^{-2})$ term in the asymptotic expansion of the spectrum of $\mathbf{M}^0$ to vanish exactly yields the condition

$$E_1 \tilde{D}_2 + E_2 \tilde{D}_1 + 2(E_2 D_{y,1} + E_1 D_{y,2}) = 0. \tag{24}$$

Computing the eigenvalues of $\mathbf{M}$ under the condition, Eq. (24), yields

$$\nu_\pm = \frac{1}{2}\left[M^0_{1,1} + M^0_{2,2} \pm \left\{\left(M^0_{1,1} - M^0_{2,2}\right)^2 + 4M^0_{1,2}M^0_{2,1} + \frac{4}{\Delta}(E_1\tilde{D}_2 + 2E_2 D_{y,1})\left(M^0_{2,1} + M^0_{2,2} - M^0_{1,1} - M^0_{1,2}\right)\right\}^{1/2}\right], \tag{25}$$

where $M^0_{j,j'}$ are the $O(1)$ terms in the elements of $\mathbf{M}^0$ as defined in Eqs. (23). Clearly this diverges at the origin as $O(r^{-1}, s^{-1})$ unless at least one of the two conditions

$$M^0_{2,1} + M^0_{2,2} - M^0_{1,1} - M^0_{1,2} = 0, \tag{26a}$$

$$E_j \tilde{D}_{j'} + 2E_{j'} D_{y,j} = 0, \quad j' \neq j = 1, 2, \tag{26b}$$

is satisfied. Substituting the definitions of $M^0_{j,j'}$ into Eq. (26a) and then separately setting the $O(r^2)$ and $O(s^2)$ terms to zero yields

$$\left(\beta^r_{2,1} + \beta^r_{2,2}\right)(\tilde{D}_1 + 2D_{y,1}) - \left(\beta^r_{1,1} + \beta^r_{1,2}\right)(\tilde{D}_2 + 2D_{y,2}) = 0, \tag{27a}$$

$$\left(\beta^s_{2,1} + \beta^s_{2,2}\right)(\tilde{D}_1 + 2D_{y,1}) - \left(\beta^s_{1,1} + \beta^s_{1,2}\right)(\tilde{D}_2 + 2D_{y,2}) = 0. \tag{27b}$$

Simplifying by solving Eqs. (27) simultaneously produces the first stability condition (1SC),

$$\tilde{D}_j \equiv D_j + 2D_{x,j} = -2D_{y,j}, \quad j = 1, 2, \tag{28}$$

since the βs are a function of the transport problem parameters, independent of the preconditioner. Alternatively, solving Eqs. (26b) simultaneously produces the second stability condition (2SC),

$$\tilde{D}_j = -2(E_j/E_{j'})D_{y,j'}, \quad j' \neq j = 1, 2. \tag{29}$$

Satisfaction of at least one of the two conditions 1SC and 2SC is necessary for the flat mode to be stable.

4. IMPOSSIBILITY OF UNCONDITIONAL STABILITY AND ROBUSTNESS

An acceleration method utilizing the cell-centered AP formalism has been developed for WDD in two-dimensional geometry and shown, using homogeneous model problem analysis and extensive numercial testing, to be stable and robust [7]. Hence, the question is not whether there is a stable and robust AP, since at least one exists; rather, the question is whether the stability and robustness illustrated in [7] are unconditional in the presence of unconstrained material discontinuities. Numerical results suggest a negative answer to this question, thereby motivating the search for another AP scheme, i.e., a different formula for the AP parameters in terms of problem specifications, that is potentially unconditionally stable and robust. The result of this section, namely the impossibility of an AP scheme that is unconditionally stable and robust, preempts such a search. It is still a fact, however, that a well-designed AP (e.g., [7]) is stable and more robust than SI for most difficult-to-converge configurations but can require an increasing number of iterations to converge as the problem is made harder. Furthermore, while it is not proven here, numerical evidence is presented in Section 5 indicating that other numerical methods for solving the discrete ordinates equations accelerated via face-centered DSA exhibit similar conditional robustness in the PHI configuration.

In order to establish the impossibility of unconditional and simultaneous stability and robustness of any cell-centered AP-type acceleration scheme we need only construct one case where no choice of the preconditioner parameters ($\tilde{D}_j$, $D_{y,j}$, $j = 1, 2$) results in a spectral radius bounded below 1 regardless of problem specifications (b_j, σ_j, α_j^x, α_j^y, $j = 1, 2$, μ, η). This is accomplished for the specific PHI configuration: $\sigma_1 = 1/\sigma_2 \equiv \sigma$, $b_1 = b_2 = \sigma^2$, in the limit $\sigma \to 0$. This limit defines a sequence of PHI problems in which the optical height of the two layers diminishes like σ^3 and σ, while the optical width in the first layer diminishes like σ and in the other layer increases like σ^{-1}. For a generic member of this sequence we focus on two particular eignemodes, $r, s \to 0$ and $r = \pi/2$, $s = 0$, and show that for both stability conditions, Eqs. (28) and (29), the condition for robustness of the former eigenmode results in asymptotic estimates of the preconditioner parameters that cause the latter eigenmode to become unstable. Since stability of an acceleration scheme is a more essential property than robustness, it follows that the most one can expect of a cell-centered AP is unconditional stability, but conditional robustness [7].

It is important for the success of the ensuing asymptotic analyses that entail two asymptotic limits, namely $r, s \to 0$ and $\sigma \to 0$, that we define the manner in which the limit points

are approached. A fixed, finite σ defines a specific PHI configuration for which the limit $r, s \to 0$ employed to derive the stability conditions in Section 3 is valid. Smaller values of σ in the sequence $\sigma \to 0$ will require considering the Fourier variables, r, s, in an ever tighter region around the origin in order for the analysis, hence the stability conditions, to remain valid. In other words, r, s must approach the origin faster than $\sigma \to 0$.

First we determine the asymptotic behavior of the various coefficients in the **B** matrix in this limit near the origin,

$$\begin{bmatrix} E_1 \\ E_2 \end{bmatrix} \to \begin{bmatrix} 1-\sigma^2 \\ \sigma^2 \end{bmatrix}, \tag{30a}$$

$$\begin{bmatrix} \beta^r_{1,1} & \beta^r_{1,2} \\ \beta^r_{2,1} & \beta^r_{2,2} \end{bmatrix} \to \begin{bmatrix} 0 & -\left(\frac{1}{3}+12\overline{\mu^2}\right)\sigma^2 \\ 0 & -\left(\frac{1}{3}+12\overline{\mu^2}\right)\sigma^2 \end{bmatrix}, \tag{30b}$$

$$\begin{bmatrix} \beta^s_{1,1} & \beta^s_{1,2} \\ \beta^s_{2,1} & \beta^s_{2,2} \end{bmatrix} \to \begin{bmatrix} -4\overline{\eta^2}+(1+12\overline{\eta^2})\sigma^2 & -4\overline{\eta^2}\sigma^{-2}+\left(\frac{1}{2}+12\overline{\eta^2}\right) \\ -4\overline{\eta^2}+\left(\frac{1}{2}+12\overline{\eta^2}\right)\sigma^2 & -4\overline{\eta^2}\sigma^{-2}+12\overline{\eta^2} \end{bmatrix}, \tag{30c}$$

where the overbar indicates a weighted sum over discrete ordinates, e.g., $\overline{\mu^2} \equiv \sum_{\mu,\eta} \omega\mu^2$, and where we have assumed perfect scattering, $c_1 = c_2 = 1$. Note that due to the assumed symmetry of the angular quadrature, $\bar{\mu} = 0$ and $\bar{\eta} = 0$. These expressions define the asymptotic behavior of the SI scheme near the origin in Fourier space for the case under consideration when $\sigma \to 0$.

Next we evaluate the **B** matrix at the eigenmode $r = \pi/2$, $s = 0$ in the limit $\sigma \to 0$ starting with the expressions for the **A** matrix derived earlier,

$$\mathbf{B}(\pi/2, 0) = \begin{bmatrix} 0 & \tilde{\mu} \\ 0 & \tilde{\mu} \end{bmatrix} + O(\sigma), \tag{31}$$

where we have defined $\tilde{\mu} \equiv \overline{(1+12\mu^2)^{-1}}$.

4.1. The First Stability Condition

Now we apply 1SC to AP and show that the robustness of the flat mode, $r, s \to 0$, results in an unbounded eigenvalue at $r = \pi/2$, $s = 0$.

4.1.1. *Robustness of the Flat Eigenmode: $r, s \to 0$*

The limit of the eigenvalues of the **M** matrix under 1SC near the origin in Fourier space is given by Eq. (25). Upon applying 1SC to Eq. (25) the $O(\Delta^{-1})$ term vanishes and the discriminant becomes a perfect square yielding the simple expression $\nu_\pm = [M^0_{1,1} + M^0_{2,2} \pm (M^0_{1,2} + M^0_{2,1})]/2$, which in the limit $\sigma \to 0$ becomes

$$\nu_- = \frac{4r^2[\sigma^2 D_{x,1} + (1-\sigma^2)D_{x,2}] + s^2[\sigma^2 D_{y,1} + (1-\sigma^2)D_{y,2}]}{8r^2(D_{x,1}D_{y,2} + D_{x,2}D_{y,1}) + 4s^2 D_{y,1}D_{y,2}}, \tag{32a}$$

$$\begin{aligned}\nu_+ = 1 + \{&2r^2\sigma^2(1+36\overline{\mu^2})(D_{y,1}+D_{y,2}) + s^2[24\overline{\eta^2}(\sigma^{-2}-2-3\sigma^2)(D_{y,1}+D_{y,2}) \\ &- 3(\sigma^2 D_{y,1} + D_{y,2}) - 6\sigma^2 D_{y,2}]\} \div \{24r^2(D_{x,1}D_{y,2} + D_{x,2}D_{y,1}) + 12s^2 D_{y,1}D_{y,2}\}.\end{aligned} \tag{32b}$$

Now we compute the leading term of ν_+ along the r- and s-axes keeping in mind that the asymptotic behavior of the preconditioner parameters with respect to σ is yet undetermined; that is, $D_{y,j} = O(\sigma^{N_{y,j}})$, $j = 1, 2$. Evaluating ν_+ along the s-axis, then collecting the coefficients of $D_{y,1}$ and $D_{y,2}$ in the numerator and allowing the $O(\sigma^{-2})$ terms to dominate higher order terms, yields

$$\nu_+ \to 1 + \frac{2\overline{\eta^2}}{\sigma^2}\left[\frac{1}{D_{y,1}} + \frac{1}{D_{y,2}}\right], \quad \text{as } s \to 0, \tag{33}$$

which diverges as $\sigma \to 0$ unless $N_{y,j} \leq -2$. Furthermore, in order to prevent a unity eigenvalue (which would imply lack of robustness of this eigenmode) it is necessary that

$$\max[N_{y,1}, N_{y,2}] = -2. \tag{34}$$

Next evaluating ν_+ along the r-axis,

$$\nu_+ \to 1 + \frac{\sigma^2(1 + 36\overline{\mu^2})(D_{y,1} + D_{y,2})}{12(D_{x,1}D_{y,2} + D_{x,2}D_{y,1})}, \quad \text{as } r \to 0, \tag{35}$$

which implies that a necessary condition for robustness is

$$\frac{(D_{y,1} + D_{y,2})}{(D_{x,1}D_{y,2} + D_{x,2}D_{y,1})} = O(\sigma^{-2}). \tag{36}$$

We now use Eqs. (34) and (36) to show that $D_{y,j}$ dominates $D_{x,j}$ for $j = 1, 2$ as $\sigma \to 0$. First we note that Eq. (36) amounts to

$$\min[N_{x,2} + N_{y,1}, N_{x,1} + N_{y,2}] = \min[N_{y,1} + 2, N_{y,2} + 2], \tag{37}$$

where $N_{x,j}$ are defined in analogy to $N_{y,j}$. Suppose by Eq. (34) $N_{y,1} \leq N_{y,2} = -2$; then in Eq. (37) either

$$\begin{aligned} &N_{x,2} + N_{y,1} \geq N_{x,1} + N_{y,2} = N_{y,1} + 2 \\ &\quad \Rightarrow N_{x,2} \geq 2 > N_{y,2} \quad \text{and} \quad N_{x,1} = N_{y,1} + 4 > N_{y,1} \end{aligned}$$

or

$$\begin{aligned} &N_{x,1} + N_{y,2} \geq N_{x,2} + N_{y,1} = N_{y,1} + 2 \\ &\quad \Rightarrow N_{x,1} \geq N_{y,1} + 4 > N_{y,1} \quad \text{and} \quad N_{x,2} = 2 > N_{y,2}. \end{aligned}$$

Hence under assumption $N_{y,1} \leq N_{y,2} = -2$ we must have

$$N_{x,j} > N_{y,j}, \quad j = 1, 2. \tag{38}$$

Analogously, if by Eq. (34) $N_{y,2} \leq N_{y,1} = -2$, the same inequality (38) is reached. We now use this inequality to show that the eigenvalue at $r = \pi/2$, $s = 0$ is $O(\sigma^{-2})$, i.e., unbounded as $\sigma \to 0$.

4.1.2. *Instability of the Eigenmode $r = \pi/2$, $s = 0$*

Substituting $r = \pi/2$, $s = 0$ in the Fourier-decomposed preconditioner operator [see Eq. (11)] and applying 1SC and inverting the resulting matrix we obtain

$$\mathbf{D}^{-1}(\pi/2, 0) \rightarrow \frac{-1}{8D_{x,1}D_{x,2} + 4D_{x,2}D_{y,1} + 4D_{x,1}D_{y,2}} \begin{bmatrix} 2D_{x,2} + D_{y,2} & D_{y,1} \\ D_{y,2} & 2D_{x,1} + D_{y,1} \end{bmatrix}. \tag{39}$$

This can be simplified in the limit $\sigma \rightarrow 0$ by using inequality (38) in the diagonal elements, and by noting that the denominator can be rewritten as

$$4D_{x,1}(D_{x,2} + D_{y,2}) + 4D_{x,2}(D_{x,1} + D_{y,1}) \sim 4(D_{x,1}D_{y,2} + D_{x,2}D_{y,1}), \tag{40}$$

due to inequality (38), to produce

$$\mathbf{D}^{-1}(\pi/2, 0) \rightarrow \frac{-1}{4(D_{x,2}D_{y,1} + D_{x,1}D_{y,2})} \begin{bmatrix} D_{y,2} & D_{y,1} \\ D_{y,2} & D_{y,1} \end{bmatrix}. \tag{41}$$

The preconditioned iterations for this eigenmode, under 1SC, are governed by

$$\mathbf{M}(\pi/2, 0) \rightarrow \begin{bmatrix} D_{y,2} & D_{y,1} - \tilde{\mu}[D_{y,1} + D_{y,2} - 4(D_{x,2}D_{y,1} + D_{x,1}D_{y,2})] \\ D_{y,2} & D_{y,1} - \tilde{\mu}[D_{y,1} + D_{y,2} - 4(D_{x,2}D_{y,1} + D_{x,1}D_{y,2})] \end{bmatrix} \div [4(D_{x,2}D_{y,1} + D_{x,1}D_{y,2})]. \tag{42}$$

Since the two rows in Eq. (42) are identical, the two eigenvalues of $\mathbf{M}(\pi/2, 0)$ are equal to zero and the sum of the elements in either row. It follows that a lower bound on the spectral radius is provided by

$$\rho_{l.b.} = \left| \tilde{\mu} + \frac{1}{4}(1 - \tilde{\mu}) \left(\frac{D_{y,1} + D_{y,2}}{D_{x,2}D_{y,1} + D_{x,1}D_{y,2}} \right) \right|. \tag{43}$$

Since $\tilde{\mu} < 1 \Rightarrow 1 - \tilde{\mu} = O(\sigma^0)$, the last term in the expression for $\rho_{l.b.}$ is $O(\sigma^{-2})$ by virtue of Eq. (36) implying instability in the limit $\sigma \rightarrow 0$. Note that the instability of this eigenmode is not a general property of AP; rather, it is a consequence of the robustness condition of the flat mode in the PHI configuration.

4.2. The Second Stability Condition

In this section we apply 2SC, Eq. (29), to AP and show that a necessary condition for the robustness of the flat mode, $r, s \rightarrow 0$, of the resulting operator produces an unbounded eigenvalue for the mode $r = \pi/2$, $s = 0$.

4.2.1. *Robustness of the Flat Eigenmode: $r, s \rightarrow 0$*

Unlike 1SC, 2SC does not produce a simple discriminant for the expressions of $\nu_{\pm}$ in the neighborhood of the origin in Fourier space. However, it is possible to obtain simple formulas for the eigenvalues along the s-axis, as follows. Substituting $r = 0$ and 2SC [Eq. (29)] into

the definition of $\mathbf{M}^0$ [Eq. (23)] results in

$$\mathbf{M^0}(0, s \to 0) \sim \begin{bmatrix} 1 - E_1 + \frac{E_2}{4D_{y,2}} - \frac{E_2\beta^s_{1,1} + E_1\beta^s_{2,1}}{2E_1 D_{y,2}} & E_1 - \frac{E_2}{4D_{y,2}} - \frac{E_2\beta^s_{1,2} + E_1\beta^s_{2,2}}{2E_1 D_{y,2}} \\ E_2 - \frac{E_1}{4D_{y,1}} - \frac{E_1\beta^s_{2,1} + E_2\beta^s_{1,1}}{2E_2 D_{y,1}} & 1 - E_2 + \frac{E_1}{4D_{y,1}} - \frac{E_1\beta^s_{2,2} + E_2\beta^s_{1,2}}{2E_2 D_{y,1}} \end{bmatrix}. \quad (44)$$

Using the asymptotic expansions of the parameters E_j and $\beta^s_{j,j'}$ [Eqs. (30)], Eq. (44) simplifies to

$$\mathbf{M}^0(0, s \to 0) \sim \begin{bmatrix} \sigma^2\left(1 + \frac{2\overline{\eta^2}}{\sigma^2 D_{y,2}}\right) & 1 + \frac{2\overline{\eta^2}}{\sigma^2 D_{y,2}} \\ \sigma^2\left(1 + \frac{2\overline{\eta^2}}{\sigma^4 D_{y,1}}\right) & 1 + \frac{2\overline{\eta^2}}{\sigma^4 D_{y,1}} \end{bmatrix}, \quad (45)$$

whose two eigenvalues are

$$\nu_+ \to 1 + 2\overline{\eta^2}\left(\frac{\sigma^{-4}}{D_{y,1}} + \frac{1}{D_{y,2}}\right), \quad (46a)$$

$$\nu_- \to 0, \quad \text{as } s \to 0, \sigma \to 0. \quad (46b)$$

In Eqs. (45) we have set $\overline{\eta/\mu} = 0$ by virtue of the assumed symmetry of the angular quadrature. (An earlier presentation [10] of the proof in this section is in error because it did not recognize that the assumed symmetry of the angular quadrature implies $\overline{\eta/\mu} = 0$ and $\bar{\mu} = 0$. While the conclusion of the proof as presented here is the same, the steps needed to reach it, and intermediate results, are different.) As in the case of 1SC, here also ν_+ diverges as $\sigma \to 0$ unless $N_{y,1} \le -4$ and $N_{y,2} \le 0$. Furthermore, in order to prevent a unity eigenvalue (which would imply lack of robustness) it is necessary that at least one equality hold; i.e.,

$$N_{y,1} = -4, \quad N_{y,2} \le 0 \quad \text{or} \quad N_{y,1} \le -4, \quad N_{y,2} = 0. \quad (47)$$

Inequality (47) automatically guarantees that $\nu_- = \mathrm{O}(\sigma^2)$. Even though a simple form of the eigenvalues along the r-axis is not available, we derive conditions amounting to the dominance of the $D_{y,j}$ coefficients over the $D_{x,j'}$ that are necessary to show that the eigenvalues at $r = \pi/2, s = 0$ are unbounded. This is accomplished by substituting $s = 0$ in the formula for the $\mathbf{M}^0$ matrix, then applying the limit $\sigma \to 0$ to obtain the simplified expression

$$\mathbf{M}^0(r \to 0, 0) = \begin{bmatrix} \sigma^2 + \frac{4D_{x,2}}{\tilde{\Delta}} & 1 + \frac{2\sigma^2(1 + 36\overline{\mu^2})D_{y,1}}{3\tilde{\Delta}} - \frac{4D_{x,2}}{\tilde{\Delta}} \\ \sigma^2 - \frac{4\sigma^2 D_{x,1}}{\tilde{\Delta}} & 1 + \frac{2(1 + 36\overline{\mu^2})D_{y,2}}{3\tilde{\Delta}} + \frac{4\sigma^2 D_{x,1}}{\tilde{\Delta}} \end{bmatrix}, \quad (48)$$

where we have defined

$$\tilde{\Delta} \equiv 8(\sigma^2 D_{x,1} D_{y,1} + \sigma^{-2} D_{x,2} D_{y,2}). \quad (49)$$

Now we define the ratio

$$\delta \equiv \frac{D_{x,1} D_{y,1}}{D_{x,2} D_{y,2}} = O(\sigma^N), \quad (50)$$

and we consider the two possibilities.

1. $N \geq -4$: In this case $(1+\sigma^4\delta) = O(\sigma^0)$ and Eq. (48) simplifies to

$$\mathbf{M}^0(r \to 0, 0) \sim \begin{bmatrix} \kappa\sigma^2 & 1 + \frac{(1+36\overline{\mu^2})}{12} \frac{\sigma^4 D_{y,1}}{D_{x,2} D_{y,2}(1+\sigma^4\delta)} \\ \sigma^2 & 1 + \frac{(1+36\overline{\mu^2})}{12} \frac{\sigma^2}{D_{x,2}(1+\sigma^4\delta)} \end{bmatrix}, \tag{51}$$

where $\kappa \equiv 1 + [2D_{y,2}(1+\sigma^4\delta)]^{-1} = 1 + O(\sigma^{-N_{y,2}}) = O(\sigma^0)$ by inequality (47). Another simplification in Eq. (51) arises from $\sigma^4\delta/2D_{y,1}(1+\sigma^4\delta) = O(\sigma^{4+N-N_{y,1}}) \to 0$, as $\sigma \to 0$, at least as fast as σ^4 by virtue of inequality (47). The eigenvalues of the matrix in Eq. (51) simplify further to

$$\nu_\pm \sim \frac{1}{2}\left[1 + \frac{(1+36\overline{\mu^2})}{12(1+\sigma^4\delta)} \frac{\sigma^2}{D_{x,2}} \pm \sqrt{\left(1 + \frac{(1+36\overline{\mu^2})}{12(1+\sigma^4\delta)} \frac{\sigma^2}{D_{x,2}}\right)^2 + \frac{(1+36\overline{\mu^2})}{3(1+\sigma^4\delta)} \frac{\sigma^6 D_{y,1}}{D_{x,2} D_{y,2}}}\right]. \tag{52}$$

We show that $N_{x,2} \leq N_{y,1} + 4$ contradicts a necessary condition for the robustness of the flat eigenmode. By this hypothesis the last term under the square root sign in Eq. (52) is of order $O(\sigma^\Lambda)$, $\Lambda = 6 + (N_{y,1} - N_{x,2}) - N_{y,2} \geq 2 - N_{y,2}$. Inequality (47) then provides that $\Lambda \geq 2$, so that this term is dominated by 1 and the eigenvalues become

$$\nu_\pm \sim 1 + \frac{(1+36\overline{\mu^2})}{12(1+\sigma^4\delta)} \frac{\sigma^2}{D_{x,2}} \quad \text{and} \quad 0. \tag{53}$$

Robustness of this eigenmode, therefore, requires that $N_{x,2} = 2$, in contradiction to the hypothesis combined with inequality (47). Hence we conclude that the condition $N_{x,2} > N_{y,1} + 4$ is necessary for robustness of the flat eigenmode. Substituting this condition into this case's hypothesis, $N \geq -4$, yields $-4 \leq N_{x,1} + (N_{y,1} - N_{x,2}) - N_{y,2} < -4 + N_{x,1} - N_{y,2}$, which implies $N_{x,1} > N_{y,2}$. Note that in allowing 1 to dominate the last term under the square root sign in Eq. (52) we assumed that the squared term is not zero; had this been the case, then $N_{x,2} = 2$ and the contradiction to the hypothesis would have arisen immediately.

2. $N < -4$: In this case $(1+\sigma^4\delta) \sim \sigma^4\delta$ and Eq. (48) simplifies to

$$\mathbf{M}^0(r \to 0, 0) \sim \begin{bmatrix} \sigma^2 & 1 + \frac{(1+36\overline{\mu^2})}{12} \frac{D_{y,1}}{\delta D_{x,2} D_{y,2}} \\ \sigma^2 & 1 + \frac{(1+36\overline{\mu^2})}{12} \frac{\sigma^{-2}}{\delta D_{x,2}} \end{bmatrix}, \tag{54}$$

where we have applied two asymptotic simplifications.

- $\sigma^{-2}/2\delta D_{y,2}$ is of order $(-2-N) - N_{y,2} > 2 - N_{y,2} \geq 2$ by inequality (47); thus this term is dominated by σ^2.
- $\sigma^{-2}/D_{y,1} = O(\sigma^{-2-N_{y,1}}) \to 0$ as $\sigma \to 0$ at least as fast as σ^2 by inequality (47); thus this term is dominated by 1 and $1/D_{y,1}$ is dominated by σ^2.

The eigenvalues of the matrix in Eq. (54) follow

$$\nu_\pm \sim \frac{1}{2}\left[1 + \frac{(1+36\overline{\mu^2})}{12} \frac{\sigma^{-2}}{\delta D_{x,2}} \pm \sqrt{\left(1 + \frac{(1+36\overline{\mu^2})}{12} \frac{\sigma^{-2}}{\delta D_{x,2}}\right)^2 + \frac{(1+36\overline{\mu^2})}{3} \frac{\sigma^2 D_{y,1}}{\delta D_{x,2} D_{y,2}}}\right]. \tag{55}$$

Again we show a contradiction if $N_{x,2} \le N_{y,1} + 4$. Under such a condition the last term under the square root sign is $O(\sigma^{\Lambda})$, $\Lambda = 2 + N_{y,1} - N - N_{x,2} - N_{y,2} \ge -2 - N - N_{y,2}$ by hypothesis, and $\Lambda \ge -2 - N$ by inequality (47). Hence by this case's condition on N we obtain $\Lambda > 2$, implying that this term is dominated by 1 and the eigenvalues, Eq. (55), become

$$\nu_{\pm} \sim 1 + \frac{(1 + 36\overline{\mu^2})}{12} \frac{\sigma^{-2}}{\delta D_{x,2}} \quad \text{and} \quad 0. \tag{56}$$

Robustness of this eigenmode requires that $N_{x,2} + N = -2 \Rightarrow N_{x,2} - 4 > -2 \Rightarrow N_{x,2} > 2$, in contradiction to the hypothesis $N_{x,2} \le N_{y,1} + 2$. Hence the condition $N_{x,2} > N_{y,1} + 2$ is necessary for the robustness of this eigenemode. The above discussion permits two possibilities.

- $N_{x,1} \ge 2$; then inequality (47) immediately produces $N_{x,1} > N_{y,2}$.
- $N_{x,1} < 2$; then the last term under the square root in Eq. (55) is of order $2 - N_{x,1} > 0$, implying that it is dominated by 1. In this case, too, it follows that $N_{x,2} + N = -2$ is necessary for robustness, and again we obtain $N_{x,1} > N_{y,2}$.

To summarize the two possibilities analyzed above, the conditions

$$N_{x,1} > N_{y,2}, \quad N_{x,2} > N_{y,1} + 4 \tag{57}$$

are necessary for the robustness of the flat eigenmode as $r \to 0$ on the r-axis. Now we use inequality (57) to show that the eigenvalue at $r = \pi/2$, $s = 0$ is unbounded.

4.2.2. *Instability of the Eigenmode $r = \pi/2$, $s = 0$*

Upon applying 2SC to the inverse of the preconditioner matrix at this eigenmode, then taking the limit $\sigma \to 0$ and using inequality (57), we obtain

$$\mathbf{D}^{-1}(\pi/2, 0) = -\frac{1}{4(\sigma^4 D_{x,1} D_{y,1} + D_{x,2} D_{y,2})} \begin{bmatrix} \sigma^4 D_{y,1} & \sigma^2 D_{y,1} \\ \sigma^2 D_{y,2} & D_{y,2} \end{bmatrix}. \tag{58}$$

The preconditioned iterations for this eigenmode are governed by

$$\mathbf{M}(\pi/2, 0) = \begin{bmatrix} \frac{\sigma^4 D_{y,1}}{4(\sigma^4 D_{x,1} D_{y,1} + D_{x,2} D_{y,2})} & \tilde{\mu} + (1 - \tilde{\mu}) & \frac{\sigma^2 D_{y,1}}{4(\sigma^4 D_{x,1} D_{y,1} + D_{x,2} D_{y,2})} \\ \frac{\sigma^2 D_{y,2}}{4(\sigma^4 D_{x,1} D_{y,1} + D_{x,2} D_{y,2})} & \tilde{\mu} + (1 - \tilde{\mu}) & \frac{D_{y,2}}{4(\sigma^4 D_{x,1} D_{y,1} + D_{x,2} D_{y,2})} \end{bmatrix}. \tag{59}$$

The supremum of the magnitude of the two eigenvalues of the matrix $\mathbf{M}(\pi/2, 0)$ is bounded from below by half the sum of its diagonal elements, which can be simplified to

$$\rho_{l.b.} = \left| \frac{\tilde{\mu}}{2} + \frac{\sigma^4 D_{y,1}[1/D_{y,2} + (1 - \tilde{\mu})/\sigma^4 D_{y,1}]}{8 D_{x,2}(1 + \sigma^4 \delta)} \right|. \tag{60}$$

Since $\tilde{\mu} < 1 \Rightarrow 1 - \tilde{\mu} = O(\sigma^0)$, and using inequality (47), we conclude that

$$\frac{1}{D_{y,2}} + \frac{1 - \tilde{\mu}}{\sigma^4 D_{y,1}} = O(\sigma^0). \tag{61}$$

For $\delta = O(\sigma^N)$ consider the two possibilities.

- $N \geq -4$; then $\sigma^4 D_{y,1}/D_{x,2} = O(\sigma^{4+N_{y,1}-N_{x,2}})$, which diverges as $\sigma \to 0$ since $N_{y,1} - N_{x,2} + 4 < 0$ by inequality (57).
- $N < -4$; then $D_{y,1}/\delta D_{x,2} = D_{y,2}/D_{x,1} = O(\sigma^{N_{y,2}-N_{x,1}})$, which also diverges as $\sigma \to 0$ by inequality (57).

In summary, necessary conditions for the stability and robustness of the flat mode result in the instability of the eigenmode $(\pi/2, 0)$ in the limit $\sigma \to 0$ of the PHI configuration.

5. NUMERICAL RESULTS

As explained in Section 1, the impetus for analyzing the iterative performance of acceleration schemes in configurations that include some form of material discontinuity arose from earlier numerical tests involving AP for WDD methods [6, 7]. These results illustrated the failure of spectral analysis of AP conducted on a standard model configuration to predict iterative performance in the presence of sharp material discontinuities. This motivated a spectral analysis of AP in the PHI configuration, which demonstrated that while sharp material discontinuity did not break the unconditional stability of AP, its robustness degraded, requiring a number of iterations that grew larger with the material discontinuity [8]. Success of the PHI configuration in predicting this behavior of AP for WDD led to extension of the analysis to a DSA scheme employed in accelerating an even-parity S_n method [11]. The conclusion of that study, supported by numerical tests, is consistent with that of the AP scheme stated above. The numerical results reported in Refs. [6, 7, 11] can be viewed as verifications of the theoretical result of this paper that goes beyond the limitations set forth; namely, they cover two different numerical methods, with two different acceleration schemes, and non-PHI configurations.

In order to more faithfully test the results of the foregoing analysis we use three discrete ordinates codes that employ a variety of numerical methods and acceleration schemes to solve a sequence of PHI problems with diminishing σ. Two caveats regarding the contents of this section are worth noting from the outset. First, this paper proves a negative result, namely that for the class of WDD methods no cell-centered preconditioner with the diffusive coupling stencil is unconditionally and simultaneously stable and robust. Clearly the correctness of this result cannot be verified using a finite set of methods. Hence, the numerical results presented here must be interpreted as a check that existing accelerated discrete ordinates codes behave as predicted by the PHI analysis, even if they are based on different numerical methods and acceleration techniques than are employed in the analysis. Second, the measured performance reported here should not be used to compare acceleration methods because the quality of the converged solutions is not necessarily the same across methods. Furthermore, one of the methods converges higher moments of the flux, not just the lowest order moment, thereby potentially implying a more stringent convergence than for the low-order methods. The only relevant information to be judged by these numerical experiments is whether the spectral radius of the methods tested attains values far above the range predicted by Fourier analysis of the homogeneous configuration.

The problem configuration employed in the tests reported below is the finite approximation of the PHI configuration depicted in Fig. 1. The material assignment to rows of cells follows the PHI pattern; i.e., odd-indexed rows are assigned material 1, even-indexed rows are assigned material 2. Both materials have a unit scattering ratio, and the total cross-sections are σ and σ^{-1} for materials 1 and 2, respectively. The problem domain is source

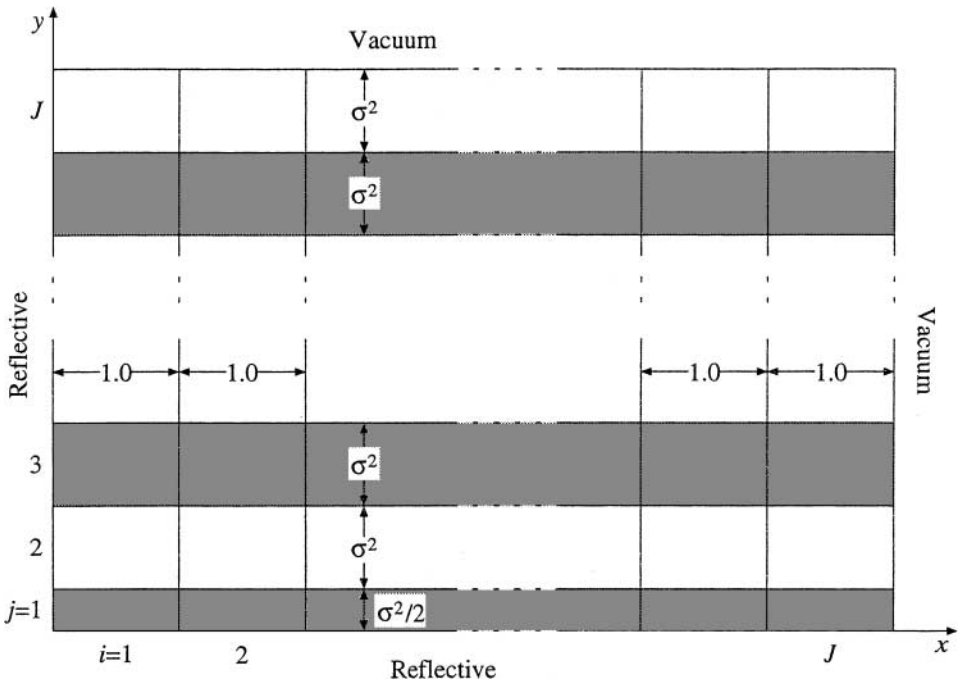

FIG. 1. Finite approximation of the PHI configuration employed in numerical tests. The total cross sections are σ_1 and σ_2, in the shaded and unshaded stripes, respectively.

free except for cell $i = 1$, $j = 1$, which contains a fixed distributed source of strength 10^9, and the angular quadrature used is S_6. The relative pointwise convergence criterion is set to 10^{-6} and the maximum number of iterations is limited to 500. Upon convergence, the spectral radius is computed as the ratio of the L_2 norm of the iterative residual in the last iterate to that in the previous iterate [13].

The test problem is solved for the sequence $\sigma = \{1/10, 1/20, 1/40, 1/80, 1/160\}$, and the sequence of meshes $J = \{10, 20, 40, 80, 160\}$. The σ sequence is in accordance with the limit examined in Section 4. The J sequence is selected to cause the optical dimensions of the entire problem to increase with increasing J, thereby reducing the effect of leakage at the right and top boundaries on the spectral properties. Furthermore, increasing J implies an increasing number of eigenmodes for the underlying iterative operators, causing its spectrum to better approximate the continuum considered in the analysis.

The first method tested is the one analyzed in this paper: the AHOT-N0 (a WDD method) accelerated with AP [7]. The spectral radius of the iterative process in the PHI configuration is presented in Table I. Note that the sequence of spectral radius values for a fixed value of σ and increasing J intuitively approximates the limit $r, s \to 0$ analyzed in the body of this paper. The decreasing spectral radius for fixed J as σ decreases is a consequence of increasing leakage at the right and top boundaries of the problem as the total optical size of the problem diminishes. The pattern of increasing spectral radius for each value of σ as J increases is a clear manifestation of the behavior predicted by the spectral analysis of the PHI configuration, particularly since the reported values of the spectral radius are much larger than expected from the spectral analysis of the homogeneous model problem [7]. To further illustrate this fact, a homogenized version of the finite PHI configuration, wherein

TABLE I
Spectral Radius of AP-Accelerated Iterations for the PHI Configuration as a Function of σ and Number of Computational Cells: AHOT-N0 Method

	σ^{-1}				
Mesh	10	20	40	80	160
10	0.100	0.039	0.010	0.002	4×10^{-4}
20	0.241	0.132	0.044	0.010	0.002
40	0.422	0.316	0.151	0.046	0.010
80	0.581	0.539	0.360	0.160	0.048
160	0.683	0.713	0.609	0.386	0.165

the same mesh structure is homogeneously covered with material 1 and separately with material 2, results in spectral radii, as shown in Tables II and III, respectively, well within the theoretically predicted range [7]. Hence these numerical tests illustrate the stability of AP for AHOT-N0 in the finite PHI configuration, albeit at a loss of unconditional robustness, in accordance with the theoretical result. By loss of *unconditional robustness* we mean that for every small $\varepsilon > 0$, there is a value of σ small enough to yield a spectral radius for the AP-accelerated AHOT-N0 equal to 1-ε, in contrast to the homogeneous configurations where the spectral radius is far smaller than 1 for all meshes and material properties.

In order to demonstrate the potential susceptibility of alternative numerical methods accelerated with schemes different from the one analyzed in this paper we conduct the same numerical tests described above using two previously reported codes. A discrete ordinates code employing a corner balance (CB) spatial differencing scheme is tested first. This code, CBP_1–DSA, uses a DSA operator based on a spatial discretization of the P_1 equations to accelerate iterative convergence [12]. In two-dimensional Cartesian geometry the resulting accelerated iterations were shown, via Fourier analysis of the homogeneous model problem congfiguration, to possess a spectral radius of 0.46 for S_2, and ≤ 0.27 for S_n, $n = 4, 8$ [12]. Numerical tests with mild material discontinuity yielded rates of convergence consistent with the analytical result. However, upon solving the finite PHI problems with CBP_1–DSA, substantial deterioration of the spectral radius is observed, as shown in Table IV, to values far larger than predicted by the homogeneous model problem spectral analysis. The pattern

TABLE II
Spectral Radius of AP-Accelerated Iterations for the Homogeneous Configuration, σ_1, as a Function of σ and Number of Computational Cells: AHOT-N0 Method

	σ^{-1}				
Mesh	10	20	40	80	160
10	2×10^{-4}	3×10^{-6}	3×10^{-8}	3×10^{-10}	3×10^{-13}
20	8×10^{-4}	2×10^{-5}	2×10^{-7}	2×10^{-9}	10^{-10}
40	0.003	8×10^{-5}	10^{-6}	10^{-8}	10^{-10}
80	0.007	3×10^{-4}	6×10^{-6}	8×10^{-8}	7×10^{-10}
160	0.015	0.001	2×10^{-5}	4×10^{-7}	4×10^{-9}

TABLE III
Spectral Radius of AP-Accelerated Iterations for the Homogeneous Configuration, σ_2, as a Function of σ and Number of Computational Cells: AHOT-N0 Method

	σ^{-1}				
Mesh	10	20	40	80	160
10	0.027	0.017	0.009	0.003	0.001
20	0.036	0.040	0.018	0.009	0.004
40	0.039	0.037	0.048	0.018	0.009
80	0.038	0.040	0.038	0.056	0.019
160	0.038	0.040	0.041	0.038	0.064

in Table IV of increasing spectral radius with increasing J for each value of σ is similar to that in Table I and is consistent with the theoretical result of the analysis in Section 4 even though the numerical method and the diffusion accelerator are corner based.

Finally, the diffusion-accelerated linear–bilinear nodal method is tested [13]. This discrete ordinates method is based on a bilinear expansion of the flux variables over a cell and is accelerated via a multilevel DSA whose variable unknowns are corner based. Thus, this method deviates from the assumptions in the analysis in two ways: the local expansion order is higher than constant, and the acceleration equations are not cell centered. Spectral analysis of this scheme on a homogeneous model configuration showed it to be unconditionally stable and robust with a spectral radius smaller than 0.63 and 0.45 for S_2 and S_n, $n \leq 4$, respectively. Nevertheless, in the finite PHI configuration this method exhibits only conditional robustness, as illustrated by the measured spectral radius reported in Table V.

The pattern of increasing spectral radius with increasing J is similar to that in Table I with two exceptions. First, a smaller value of the spectral radius is observed for the case $J = 160$, $\sigma = 1/20$ than for all neighboring points in the table. We conjecture that this is an anomaly in the L_2 norm of the error not indicative of the true spectral radius of the iterative procedure, which converged after 388 iterations, inconsistent with the value 0.392 and the 10^{-6} convergence criterion. Second, the cases with $\sigma \leq 1/80$ diverge; most likely this divergence is numerical in nature resulting from numerical imprecision noise, not a genuine property of the acceleration scheme.

TABLE IV
Spectral Radius of DSA-Accelerated Iterations for the PHI Configuration as a Function of σ and Number of Computational Cells: CBP_1–DSA Method

	σ^{-1}				
Mesh	10	20	40	80	160
10	0.336	0.219	0.113	0.053	0.025
20	0.495	0.385	0.233	0.117	0.055
40	0.664	0.563	0.409	0.238	0.119
80	0.807	0.724	0.608	0.422	0.242
160	0.890	0.853	0.770	0.631	0.431

TABLE V
Spectral Radius of DSA-Accelerated Iterations for the PHI Configuration as a Function of σ and Number of Computational Cells: BLN Method

	σ^{-1}				
Mesh	10	20	40	80	160
10	0.355	0.254	0.192	D[a]	D
20	0.543	0.417	0.317	D	D
40	0.717	0.607	0.452	D	D
80	0.836	0.668	0.624	D	D
160	0.901	0.392	0.671	D	D

[a] D, Iterations diverged, causing overflow.

6. CONCLUSION

We have shown that there exists no preconditioner with the AP cell-centered coupling stencil that is unconditionally and simultaneously stable and robust for weighted-difference particle transport methods. The only conditions applied to derive this result for the AHOT-N0 are the two stability conditions (one at a time) and the robustness of the flat mode. If the latter condition is not imposed, i.e., if the eigenvalue near the origin in Fourier space is allowed to approach unity as $\sigma \to 0$, as indeed is the case with the reciprocal-averaging mixing formula, then the $r = \pi/2$, $s = 0$ mode's eigenvalue remains finite. Hence, we conclude that in the context of the PHI analysis reciprocal-averaging mixing provides as small a lower bound on the spectral radius, 1, as can be achieved in the limit $\sigma \to 0$. Numerical tests that demonstrate the unconditional stability, but conditional robustness of AP attest to this fact.

In retrospect, this result should not be too surprising since by physical arguments it is known that the diffusion approximation does not hold where the flux is highly anisotropic. In the PHI configuration considered in this work, as $\sigma \to 0$, one of the layers becomes optically thick while the other layer approaches a void, producing severe anisotropy in the angular flux near the interface.

This result should not be misinterpreted as implying the worthlessness of preconditioning, e.g., DSA. Indeed there is ample evidence in the literature on the significant acceleration achieved with diffusion-like preconditioners compared to unaccelerated source iterations. In fact the PHI analysis presented here illustrates that in a perfectly scattering medium, while for any finite σ the spectral radius of SI is 1, the spectral radius of AP is bounded below 1. As $\sigma \to 0$ this lower bound approaches 1, but still this is better than SI for any practically realizable $\sigma > 0$.

The correct interpretation of the result reached here is that unconditionally and simultaneously stable and robust preconditioners of the diffusive type may exist only in one-dimensional geometry, and in multidimensional configurations with *mild* material discontinuities. From the practical point of view this interpretation can lead to further development along two possible directions:

1. Construction of novel unconditionally stable and robust preconditioners with coupling stencils that go beyond the traditionally diffusive pattern.

2. Construction of preconditioners that are conditionally stable and robust for specific problem classes, and that are easier to invert (solve) than the diffusion operator.

ACKNOWLEDGMENT

The author expresses his gratitude to Dr. Todd Wareing of Los Alamos National Laboratory for providing a copy of his BLN code, and for conducting the numerical tests with his CBP_1–DSA code and communicating the results for inclusion in this paper.

REFERENCES

1. W. H. Reed, The effectiveness of acceleration techniques for iterative methods in transport theory, *Nucl. Sci. Eng.* **45**, 245 (1971).
2. R. E. Alcouffe, Diffusion synthetic acceleration methods for the diamond-differenced discrete ordinates equations, *Nucl. Sci. Eng.* **64**, 344 (1977).
3. E. W. Larsen, Unconditionally stable diffusion synthetic acceleration methods for the slab geometry discrete ordinates equations. Part I: Theory, *Nucl. Sci. Eng.* **82**, 47 (1982).
4. M. L. Adams and E. W. Larsen, Fast iterative methods for discrete-ordinates particle transport calculations, *Prog. Nucl. Energy* **40**, 3 (2002).
5. Y. Y. Azmy, Iterative convergence acceleration of neutral particle transport methods via adjacent-cell preconditioners, *J. Comput. Phys.* **152**, 359 (1999).
6. Y. Y. Azmy, Adjacent-cell preconditioners for accelerating multidimensional neutron transport methods, in *Proceedings, Conference on Advances and Applications in Radiation Protection and Shielding, N. Falmouth, MA, April 21–25, 1996* (Am. Nucl. Soc., La Grange Park, IL, 1996), Vol. 1, p. 390.
7. Y. Y. Azmy, Acceleration of multidimensional discrete ordinates methods via adjacent-cell preconditioners, *Nucl. Sci. Eng.* **136**, 202 (2000).
8. Y. Y. Azmy, Analysis and performance of adjacent-cell preconditioners for accelerating multidimensional transport calculations, in *Proceedings, OECD/NEA Meeting on 3D Deterministic Radiation Transport Computer Programs, Features, Applications, and Perspectives, Paris, France, December 2–3, 1996* (Organization for Economic Cooperation and Development, Paris, 1997), p. 197.
9. Y. Y. Azmy, The weighted diamond difference form of nodal transport methods, *Nucl. Sci. Eng.* **98**, 29 (1988).
10. Y. Y. Azmy, Impossibility of unconditional stability and robustness of diffusive acceleration schemes, in *Proceedings, 1998 ANS Topical Meeting on Radiation Protection and Shielding, Nashville, TN, April 19–23, 1998* (Am. Nucl. Soc., La Grange Park, IL, 1998), Vol. 1, p. 480.
11. Y. Y. Azmy, T. Wareing, and J. Morel, Effect of material heterogeneity on the performance of DSA for even-farity S_n methods, in *Proceedings, 1999 ANS Topical Meeting on Mathematics and Computation, Madrid, Spain, September 27–30, 1999* (Senda Editorial, Madrid, 1999), Vol. 1, p. 55.
12. T. A. Wareing, New diffusion-synthetic acceleration methods for the SN equations with corner balance differencing, in *Proceedings of the Joint International Conference on Mathematical Methods and Supercomputing in Nuclear Applications, Karlsruhe, Germany, April 19–23, 1993* (Kernforschungszentrum, Karlsruhe, Germany, 1993), Vol. 2, p. 500.
13. T. A. Wareing, W. F. Walters, and J. E. Morel, Diffusion-accelerated solution of the two-dimensional X-Y S_n equations with linear-bilinear nodal differencing, *Nucl. Sci. Eng.* **118**, 122 (1994).